Electron Heating and Current Drive by Mode Converted Slow Waves

R. Majeski, C. K. Phillips, and J. R. Wilson
Princeton Plasma Physics Laboratory, P.O. Box 451, Princeton, New Jersey 08543
(Received 10 December 1993; revised manuscript received 8 August 1994)

An approach to obtaining efficient single-pass-mode conversion at high parallel wave number from the fast magnetosonic wave to the slow ion Bernstein wave, in a two-ion species tokamak plasma, is described. The intent is to produce localized electron heating or current drive via the mode-converted slow wave. In particular, this technique can be adapted to off-axis current drive for current profile control. Modeling for the case of deuterium-tritium plasmas in TFTR is presented.

PACS numbers: 52.50.Gj, 52.55.Fa

Mode conversion from the fast magnetosonic wave to the slow ion Bernstein wave (IBW) in a two-ion component plasma is known to play a part in ion cyclotron range of frequency (ICRF) heating schemes in tokamak plasmas. For example, mode conversion is predicted to be an important process in deuterium-tritium (D-T) plasmas [1]. In experiments with a fast wave antenna on the high-field side of the torus, IBW heating of electrons dominated the power flow [2]. Mode conversion and the modification of the fast wave polarization near the ion-ion hybrid resonance is known to be important in minority ion heating, especially at low-parallel wave number ($k_\parallel$) [1,3–7].

Most large tokamaks have high-power long-pulse ICRF systems for heating, with antennas sited on the low-field side of the torus. Here we discuss a regime for efficient fast wave—IBW mode conversion in a two-ion species plasma, for direct electron heating or current drive by the IBW using existing ICRF systems. For near-equal ion concentrations the mode-conversion surface can be sited in the plasma core, while the ion cyclotron resonances are off axis in the colder regions of the plasma to minimize ion heating. Efficient mode conversion is predicted at high $k_\parallel$ for the proper choice of plasma parameters, so that the Bernstein wave phase velocity $v_\phi = \omega/k_\parallel$ is on the order of or less than the electron thermal velocity v_{Te}. Strong, localized electron damping of the Bernstein wave is expected to result.

An examination of the cold plasma resonance and cutoff surfaces shows that, for parameters typical of large present-day tokamaks, these surfaces coalesce into a closely spaced cutoff-resonance-cutoff triplet near some experimentally accessible $k_\parallel \equiv k_{\parallel c}$. The effect of such a triplet on mode-conversion efficiency has been discussed for the Alfvén resonance [4,8,9], but the importance of the high-field-side cutoff in mode conversion at the ion-ion hybrid layer has not been previously noted. Here we model for the first time the effect of a cutoff-resonance-cutoff triplet on mode conversion in the experimentally important ion-ion hybrid case. Numerical results indicate that in excess of 80% per pass of the fast-wave power incident on the triplet can be mode converted and coupled directly to electrons.

Efficient, off-axis heating of thermal electrons has potential applications in magnetohydrodynamics (MHD) control, current profile control, and electron heat transport studies. Off-axis current drive is also of interest. Electron cyclotron heating could in principle provide a (proven) alternate bulk electron heating and current drive technique, but there are at present no microwave sources capable of supplying multimegawatt long pulse power at appropriate frequencies. In contrast, all of the present generation of large tokamaks have high power heating systems in the ICRF. High efficiency mode conversion therefore has the potential for wide utilization in the near term.

Cold plasma considerations.—For the ICRF the relevant cold plasma dispersion relation may be written [4]

$$n_\perp^2 = \frac{(K_\perp + K_x - n_\parallel^2)(K_\perp - K_x - n_\parallel^2)}{K_\perp - n_\parallel^2} = \frac{(R - n_\parallel^2)(L - n_\parallel^2)}{S - n_\parallel^2}, \quad (1)$$

where

$$K_\perp = 1 - \sum_j \frac{\omega_{pj}^2}{\omega^2 - \Omega_j^2}, \qquad K_x = \sum_j \frac{\Omega_j}{\omega} \frac{\omega_{pj}^2}{\omega^2 - \Omega_j^2},$$

and $n_\perp = ck_\perp/\omega$, $n_\parallel = ck_\parallel/\omega$, $\omega p_j^2 = nq_j^2/m_j\varepsilon_0$, $\Omega_j = q_jB_0/m$; m_j and q_j being the mass and charge of the jth species. The notation R, L, and S follow Stix [4]. Mode conversion between the fast and slow modes occurs at the $n_\parallel^2 = S$ surface when hot plasma effects are included [1]. For a plasma with two-ion species, the condition is obtained at a frequency intermediate to the two-ion cyclotron frequencies and is referred to as the ion-ion hybrid resonance.

In the situation usually considered, where $k_\parallel$ is small and the fast wave is incident from the low-field side, the fast wave is cutoff at the $n_\parallel^2 = L$ surface before reaching the resonance. The $n_\parallel^2 = R$ cutoff surface occurs at low density far from the resonance, and so the L and S surfaces form an isolated cutoff-resonance pair. In this case the mode converted power can be shown to be given by $|T|^2(1 - |T|^2)$, where $|T| = e^{-\eta}$ and η is the tunneling factor [5,6,10].

 0031-9007/94/74(16)/2204(4)$06.00

We consider here a two-ion hybrid resonance regime where the $n_\parallel^2 = L$, R, and S surfaces occur in a closely spaced cutoff-resonance-cutoff triplet. Such a situation can be produced in large tokamaks in D-T plasmas by correctly choosing the species fraction, normalized frequency, and central density. We take TFTR as an example system. In Fig. 1 a map of the locations in the equatorial plane of the cold plasma cutoffs and resonances for TFTR as a function of the parallel wave number are shown. The density profile was modeled as $n_e(r) \sim n_e(0)[1 - (r/a)^{1.5}]^{1.5}$, appropriate to a supershot discharge, with $n_e(0) = 5 \times 10^{19}$ m^{-3}, major radius 2.62 m, minor radius 0.98 m, and a central toroidal field of 4.8 T. The assumed concentration of tritium was $\eta_T \equiv n_T/n_e = 0.4$ in a deuterium plasma and the frequency 33 MHz. The cutoffs and resonances coalesce at R(major radius)~2.3 m or $r/a \sim 0.3$, for $k_\parallel = k_{\parallel c} \sim 12$ m^{-1}. This wave number is slightly higher than the peak in the vacuum antenna spectrum for the TFTR ICRF antennas, for 90° phasing, when toroidicity ($k_\parallel \sim 1/R$) is included. For $k_\parallel < k_{\parallel c}$, the ordering of the cutoffs and resonances is the same as for the familiar minority ion heating regime; for $k_\parallel > k_{\parallel c}$, the ordering is the same as for the Alfvén regime [4,8]. For $k_\parallel = k_{\parallel c}$ a cutoff is produced. In practice, $k_\parallel < k_{\parallel c}$ is required for good antenna coupling at the low-field-side edge. Two factors favor efficient mode conversion for $k_\parallel$ on the order of (but less than) $k_{\parallel c}$: the proximity of the $n_\parallel^2 = L$ cutoff and the $n_\parallel^2 = S$ resonance which allows efficient tunneling through the evanescent layer, and the second cutoff at $n_\parallel^2 = R$ which reflects transmitted fast-wave power back into the resonance from the high-field side.

The resonance location is primarily determined by the frequency and the relative concentration of the ion species, and so off-axis electron heating and current drive is possible. In fast-wave direct electron heating and current drive, by contrast, the inverse damping length of the fast wave on electrons Im$(k_\perp)$ scales as Re$(k_\perp)\beta e \xi e^{-\xi^2}$, where βe is the electron beta and $\xi = \omega/k_\parallel v_{Te}$ [11]. Hence, the power deposition profile is always peaked on axis.

In the mode-conversion case, the radial location of the power deposition can be varied with the frequency. In the limit where $n_\parallel^2 \gg 1$ but $\omega_{pi}^2 \gg n_\parallel^2 \omega^2$ the location of the resonance in major radius may be approximated as

$$R = \frac{1}{\omega}\frac{eB_0R_0}{m_1}\left[\frac{\omega_{p2}^2 + \omega_{p1}^2\mu_{\rm rel}^2}{\omega_{p1}^2 + \omega_{p2}^2}\right]^{1/2}, \qquad (2)$$

where R_0 is the major radius of the axis, B_0 is the on-axis toroidal field, and $\mu_{\rm rel}$ is ratio of the ion masses. Since $R \sim 1/\omega$ here, a 10% variation in the frequency of the coupled fast wave would vary the location of the resonance and the resulting heating or current drive, by $\Delta r/a \sim 0.25$ for typical tokamak aspect ratios. Active profile control in future long-pulse tokamaks may therefore be possible.

Mode conversion efficiency.—In the absence of the secondary high-field-side cutoff, the mode conversion efficiency is determined by the tunneling factor, which can be approximated in plane geometry as [7,8]

$$\eta = \frac{-(\pi/2)D_0^2/S'}{[-(D^2)'/S']^{1/2}}. \qquad (3)$$

Here $D = \frac{1}{2}(R - L)$ and the subscript 0 denotes evaluation at the spatial position of the $n_\parallel^2 = S$ resonance. S and D^2 have been linearized in the spatial coordinate x as $S - n_\parallel^2 = S'x$ and $D^2 = D_0^2 + (D^2)'x$, where x, y, and z, respectively, denote the radial, poloidal, and toroidal directions and are normalized to c/ω.

In Fig. 2 we plot the estimate of the percentage of the mode converted power $|T|^2(1 - |T|^2)$, $|T| = e^{-\eta}$ as a function of $k_\parallel$, using Eq. (3) to determine η. Plasma parameters were the same as for Fig. 1. Also shown in

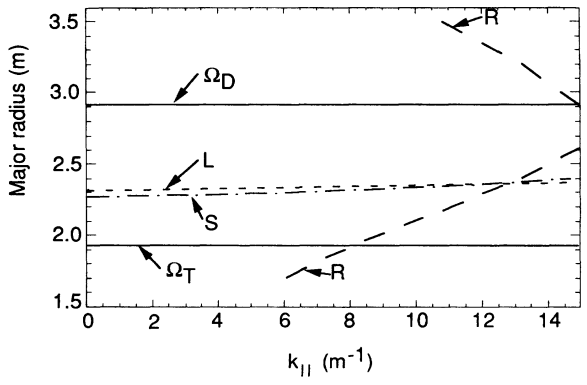

Fig. 1. Map of the cold plasma cutoff and resonant surfaces in $k_\parallel$ and major radius for TFTR. L denotes the $n_\parallel^2 = L$ cutoff, S denotes the $n_\parallel^2 = S$ resonance, and R denotes the $n_\parallel^2 = R$ cutoff. The fundamental cyclotron resonances of deuterium and tritium are indicated by Ω_D and Ω_T.

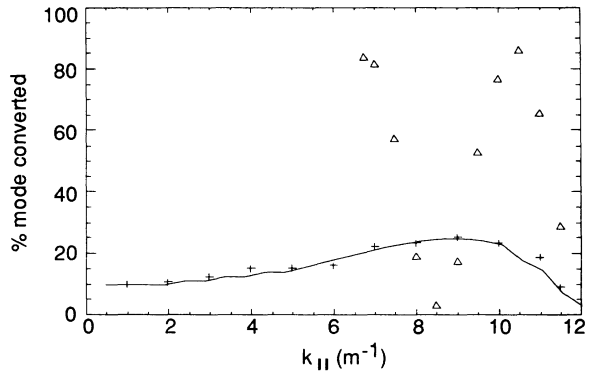

FIG. 2. Estimates of the percentage of incident power which is mode converted. The solid line denotes the analytic estimate obtained using Eq. (3) for the isolated cutoff-resonance case. The crosses indicate the numerical results obtained with the 1D code CARDS for the same case. The triangles indicate the numerical results for the mode-converted power fraction when the additional high-field-side cutoff is included.

Fig. 2 is an estimate of the mode-converted power using the fourth order 1D full wave code CARDS [12]. Here the spatial extent of the plasma slab modeled included the $n_\parallel^2 = L$ cutoff and $n_\parallel^2 = S$ resonance only; the high-field-side $n_\parallel^2 = R$ cutoff was excluded. Competing absorption mechanisms are not considered. The numerical modeling assumed a central ion temperature $T_i(0) = 20$ keV and a central electron temperature $T_e(0) = 10$ keV, with a profile varying as $T_{i,e}(0)[1 - (r/a)^{1.5}]^{2.5}$ appropriate to a supershot discharge in TFTR. For this case the analytic expression for the mode-converted power and the numerical results are in excellent agreement. Both indicate a broad maximum in the mode-conversion efficiency at $k_\parallel = 8$–$10\ \mathrm{m}^{-1}$ or somewhat below $k_{\parallel c}$.

If the $n_\parallel^2 = R$ cutoff is included, it has been shown that the mode converted power can be written as

$$P_c = \pi(D_0^2/S')|E_y|^2, \tag{4}$$

where $|E_y|$ is the y (poloidal) component of the electric field at the resonance [8]. The presence of a nearby cutoff would be expected to modify the mode-conversion efficiency by modifying $|E_y|$ at the resonance. Note that, unlike the case of a nearby conducting wall [8], $|E_y|$ does not vanish at the cutoff. The result of numerical modeling with the CARDS code in which the high-field-side $n_\parallel^2 = R$ cutoff is included is also shown in Fig. 2. For high $k_\parallel$ (9–$11.5\ \mathrm{m}^{-1}$) the mode-conversion efficiency is predicted to be significantly increased by the inclusion of the high-field-side cutoff. For this range in wave number the distance between the $n_\parallel^2 = R$ cutoff and the mode-conversion layer is less than one-half the radial wavelength of the transmitted fast wave, where the proximity of the cutoff significantly increases the wavelength. The increase in the mode-conversion efficiency scales as $|E_y^c|^2/|E_y|^2$, where $|E_y^c|$ ($|E_y|$) is numerically determined with (without) the high-field-side cutoff. The effect of a standing-wave pattern in $|E_y|$ due to reflection at the high-field-side cutoff is further evidenced by the elimination of mode conversion for $k_\parallel = 8.5\ \mathrm{m}^{-1}$. This value of the wave number is associated with a null in $|E_y|$ at the $n_\parallel^2 = S$ resonance. The full width at half maximum (FWHM) of the region in parallel wave number where the enhanced mode conversion obtained is smaller than the FWHM of the TFTR ICRF antenna spectrum but is of the same order as the predicted spectral width of antennas designed for fast-wave current drive [13]. Note that $k_\perp \rho_i < 1$ within the region of power deposition. Numerical modeling with the inclusion of the high-field-side cutoff for $k_\parallel < 6.75\ \mathrm{m}^{-1}$ could not be performed due to the proximity of the tritium cyclotron resonance.

The power deposition profile calculated using CARDS for the case discussed in relation to Figs. 1 and 2 is shown in Fig. 3. A wave number of $k_\parallel = 10\ \mathrm{m}^{-1}$ is assumed. The code boundaries include the fundamental ion cyclotron resonance of deuterium. However, because of the high-deuterium concentration, there is only 10% single-pass absorption of the incident fast wave on the deuterium, despite the 20 keV ion temperature. 20% of the incident power is reflected, with the remainder (70%) undergoing mode conversion and absorption on the electrons at $r/a \sim 0.4$ on the high-field side of the axis. The radial location of power deposition is a few cm to the high-field side of the $n_\parallel^2 = S$ layer. The FWHM of the power deposition profile is 6 cm.

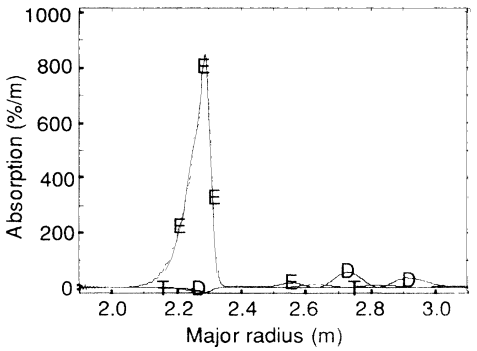

FIG. 3. Power deposition profiles computer with CARDS. Electron absorption is indicated by E, deuterium absorption by D, and tritium absorption (negligible) by T. The plasma axis is at 2.62 m.

Single-pass absorption efficiency is less dependent on the electron temperature than in the case of direct electron heating by fast waves. Numerical results with variation of the central electron temperature from 2 to 30 keV, while keeping all other parameters constant, indicate that the mode-converted power flow to electrons varies by less than 5% over this range in T_e. The power deposition profile does, however, broaden as T_e is reduced, from a FWHM value of 5 cm at $T_e(0) = 30$ keV to 20 cm at 2 keV. Direct electron damping of the fast wave (which should peak at $x = 0$) is, by contrast, negligible at 2 keV and is predicted to increase to only 4% per pass at 30 keV.

The increase in mode-conversion efficiency which results from the presence of the secondary high-field-side cutoff is further demonstrated in Fig. 4. Figure 4 is a plot of the numerically estimated absorbed, reflected, and transmitted wave power, using CARDS, as a function of the position of the high-field-side boundary. The low-field-side (source) boundary is located at $R = 3.0$ m, the $n_\parallel^2 = L$ cutoff and adjacent $n_\parallel^2 = S$ resonance are located at $R \approx 2.35$ m, and the $n_\parallel^2 = R$ cutoff is located at $R = 2.15$ m. As the absorbing boundary is moved through the $n_\parallel^2 = L$ and S surfaces the reflected power increases to approximately 25%, and a similar fraction of the power is mode converted and coupled to the electrons. As the $n_\parallel^2 = R$ cutoff is traversed the transmitted power drops to zero while the mode-converted power absorbed on electrons increases due to fast-wave reflection from the cutoff and the resultant increased electric field at the mode-conversion surface. The high predicted mode-conversion efficiency is due to inclusion of the full resonance-cutoff-resonance triplet in the modeling region.

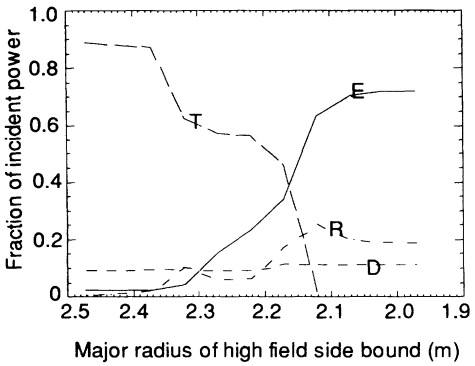

FIG. 4. Absorbed, reflected, and transmitted power as a function of the spatial position of the high-field-side boundary of the modeled region. E denotes power absorbed on electrons, D indicates deuterium absorption, R indicates reflected power, and T denotes power transmitted to the boundary.

Current drive efficiency.—For plasma parameters of interest in near-term tokamaks the coalescence of the cutoff and resonant surfaces will occur at relatively large $k_\parallel$ and, hence, low v_ϕ. The example TFTR case discussed in conjunction with Fig. 3 has $v_\phi v_{Te} \sim 0.5$ in the deposition region. With power deposition on the high-field side of the axis, the reduction of current drive efficiency due to trapped electron effects is minimized [14]. We estimate the driven current for the example case using the Ehst-Karney parameterization [14] for the current drive efficiency. All power is assumed to be deposited at an inverse aspect ratio $\varepsilon = 0.1$. Since the single-pass absorption is high, 90% of the launched fast-wave power will be deposited on electrons in a few passes. Assuming a Z_{eff} of 2, the driven current is estimated to be 0.07 A/W of coupled fast-wave power. Landau damping of the IBW is assumed. The figure of merit for current drive efficiency $\gamma \equiv (\bar{n}_e R_T/10^{20})(I/P_{\text{rf}}) = 0.06$ A W^{-1} m^{-2}.

For high parallel phase velocity waves ($N_\parallel \equiv ck_\parallel/\omega = 0.1$) the magnitude and sign of the Bernstein parallel wave number is predicted to change as the wave propagates, when poloidal field effects are included [15]. Without resorting to a fully toroidal hot plasma treatment, we can estimate the change in $k_\parallel$ due to poloidal field effects before the Bernstein wave is damped in our low phase velocity ($N_\parallel = 15$) case, using the CARDS results. At the mode-conversion surface, the Bernstein wave vector lies in the direction of decreasing major radius ($\mathbf{k} \cong -\mathbf{k}_x$, where x is the major radial direction). For propagation in the plasma midplane the parallel wave number is preserved [15]. Above or below the midplane the parallel wave number will undergo an upshift or downshift, depending on the sense of the rotational transform. In a poloidal magnetic field, $k_\parallel = k_\Theta (B_\Theta/B) + n(B_\Phi/B)/(R + r\cos\Theta)$ [15], where k_Θ denotes the projection of the Bernstein wave number onto the poloidal direction, B_Θ denotes the poloidal and B_Φ the toroidal field, Θ is the poloidal angle, and n is the toroidal mode number. For the example case, 90% of the power in the Bernstein wave is damped with $k_x < 200$ m^{-1}. Assuming that the mode-conversion layer (at $r/a = 0.4$) is located near the $q = 2$ surface, then within ± 15 cm vertical displacement from the midplane poloidal effects will cause less than a 50% change in the IBW parallel wave number before the wave is damped. Thus for mode conversion at low-phase velocity (high $k_\parallel$), in a sufficiently dense plasma for good wave focusing to occur, poloidal effects are not expected to dominate.

In conclusion, a regime for efficient excitation of the ion Bernstein wave via mode conversion of the fast magnetosonic wave for values of the launched wave number somewhat less than $k_{\parallel c}$, where $k_{\parallel c}$ denotes the wave number at which the $n_\parallel^2 = L$, R, and S surfaces coalesce, is discussed. This regime is a suitable candidate for on- or off-axis direct heating of electrons, and on- or off-axis current drive, to provide current profile control in the present generation of large tokamaks, using existing ICRF systems. Predicted off-axis current drive efficiency is approximately 0.07 A W^{-1} for typical TFTR parameters.

The authors acknowledge many useful conversations with E. F. Jaeger and P. Bonoli. CARDS was developed by D. Smithe. A. Bers, R. Hawryluk, J. Hosea, and M. Murakami all provided useful insight. This work was supported by U.S. Department of Energy Contract No. DE-AC02-76-CHO-3073.

[1] F. W. Perkins, Nucl. Fusion **17**, 1197 (1977).
[2] Equipe TFR, in *Plasma Physics and Controlled Nuclear Fusion Research,* Proceedings of the 9th Conference on Plasma Physics and Controlled Nuclear Fusion, Baltimore, 1982 (International Atomic Energy Agency, Vienna, 1983), Vol. 2, p. 17.
[3] M. Brambilla and T. Krucken, Nucl. Fusion **28**, 1813 (1988).
[4] T. H. Stix, *Waves in Plasmas* (American Institute of Physics, New York, 1992).
[5] D. G. Swanson, Phys. Fluids **28**, 2645 (1985).
[6] V. Fuchs and A. Bers, Phys. Fluids **31**, 3702 (1988).
[7] J. Jacquinot, B. D. McVey, and J. E. Scharer, Phys. Rev. Lett. **39**, 88 (1977).
[8] J. A. Heikkinen, T. Hellsten, and M. J. Alava, Nucl. Fusion **31**, 417 (1991).
[9] C. F. F. Karney, F. W. Perkins, and Y.-C. Sun, Phys. Rev. Lett. **42**, 1621 (1979).
[10] M. J. Alava and J. A. Heikkinen, Physica Scripta **45**, 345 (1992).
[11] M. Porkolab, in *Radio Frequency Power in Plasmas—1991,* Proceedings of the Ninth Topical Conference, AIP Conf. Proc. No. 244 (AIP, New York, 1991), p. 197.
[12] D. N. Smithe, Ph.D. thesis, University of Michigan, 1987.
[13] D. W. Swain, *et al.,* in *Radio Frequency Power in Plasmas—1993,* Proceedings of the Tenth Topical Conference, AIP Conf. Proc. No. 289 (AIP, New York, 1993), p. 1371.
[14] D. A. Ehst and C. F. F. Karney, Nucl. Fusion **31**, 1933 (1991).
[15] A. K. Ram and A. Bers, Phys. Fluids B **3**, 1059 (1991).